Journal of *Marine Science and Engineering*

MDPI

Article

Stability on the Excavation Surface of Submarine Shield Tunnel Considering the Fluid–Solid Coupling Effect and the Equivalent Layer

Qian Wang [1], Qiang Li [2,*], Jiancai Zhu [3,4] and Ze'an Zhu [1]

[1] School of Naval Architecture & Maritime, Zhejiang Ocean University, Zhoushan 316022, China; wangqian@zjou.edu.cn (Q.W.); zhuzean@zjou.edu.cn (Z.Z.)
[2] Department of Civil Engineering, Zhejiang Ocean University, Zhoushan 316022, China
[3] Center for Balance Architecture, Zhejiang University, Hangzhou 310027, China; zjc2009668@126.com
[4] Architectural Design and Research Institute, Zhejiang University, Hangzhou 310027, China
* Correspondence: qiangli@zjou.edu.cn; Tel.: +86-13750728926

Abstract: The support pressure on an excavation surface is a critical factor in the ground deformation and excavation stability of a submarine shield tunnel. The shield tail gap and the disturbance zone of grouting behind the tunnel wall are also important influencing factors. However, the effects of these factors on excavation stability are difficult to quantify. Consequently, a homogeneous, elastic, and annular equivalent layer is employed to simulate the thin layer behind the tunnel wall. Using COMSOL Multiphysics software, the effects of the water level depth, the thickness of the equivalent layer, the diameter of the shield tunnel, and the internal friction of soil and tunnel burial depth on the excavation deformation and ground surface subsidence of a submarine tunnel are considered with regard to the fluid–solid coupling effect. The result show that the surface subsidence of the case with respect to the fluid–solid coupling effect and the equivalent layer is larger than that without interstitial fluid and the equivalent layer, indicating that the present model can better simulate the stability of tunnel excavation. Therefore, it is important to consider the impact of the fluid–solid coupling effect and the equivalent layer on the deformation of the excavation face and ground surface subsidence.

Keywords: equivalent layer; submarine shield tunnel; fluid–solid coupling effect; excavation surface stability; support pressure ratio; ground surface subsidence

check for updates

Citation: Wang, Q.; Li, Q.; Zhu, J.; Zhu, Z. Stability on the Excavation Surface of Submarine Shield Tunnel Considering the Fluid–Solid Coupling Effect and the Equivalent Layer. *J. Mar. Sci. Eng.* **2023**, *11*, 1667. https://doi.org/10.3390/jmse11091667

Academic Editor: Cristiano Fragassa

Received: 4 July 2023
Revised: 16 August 2023
Accepted: 21 August 2023
Published: 25 August 2023

Copyright: © 2023 by the authors. Licensee MDPI, Basel, Switzerland. This article is an open access article distributed under the terms and conditions of the Creative Commons Attribution (CC BY) license (https://creativecommons.org/licenses/by/4.0/).

1. Introduction

With the development of the transportation industry in China, more and more submarine tunnels have been built in recent years. The shield tunneling method is the most popular method in tunnel construction. However, these projects have been accompanied by many engineering accidents, especially the instability of the excavation face and the deformation of excessive soil due to an inadequate support pressure ratio [1–3]. Because submarine tunnels are deeply submerged beneath the sea, the seepage effect inevitably has a significant impact on the stability of the excavation [4–6]. Even a slight mishandling can result in accidents such as excavation face collapse and water inrush [7].

So far, many scholars have conducted extensive research on the stability of tunnel excavation under seepage conditions. However, limited studies have focused on the coupling effect of fluid–solid interaction on the stability of tunnel excavations [8–11]. Ahmed et al. [12], Atkinson et al. [13], and Hisatake et al. [14] described the failure modes of shield tunnel excavation using centrifuge model tests for tunnels in homogeneous sandy soil; they obtained the ultimate support pressure in the excavation face for a collapse in tunnels, but ignored the effect of the lining. Anagnostou et al. [15–17] and Alagha et al. [18] analyzed the effect of groundwater seepage on the stability of excavation faces based on a limit analysis of tunnel excavation, and concluded that in clayey, low-permeability

soils, it is valid to perform undrained analyses during excavation, whereas drainage analyses are applicable for sandy soil. Vermeer et al. [19], Broere et al. [20], and others performed stability analysis of excavation faces under drained conditions using finite element techniques, and concluded that the pore water pressure is the significant factor on the stability of the tunnel excavation surface in which the effects of the actual soil layers and grouting conditions around the lining are neglected. Kim et al. [21] and Mair et al. [22] investigated the effects of the tunnel diameter, lateral earth pressure, and shear strength parameters of soil on the stability of excavation faces under drained conditions. They analyzed excavation surface damage with a chimney-like shape in homogeneous sandy soil strata, but the case under composite strata was ignored. Kirsch et al. [23] also applied finite element software to analyze the excavation stability of shield tunnels in dry sand; however, their studies are still limited to the case in a single sand layer. Lambrughi et al. [24] and Lü et al. [25] used FLAC3D software to analyze the stability of shield tunnel excavation faces under drained conditions and found a relationship between the support pressure and the groundwater level; accordingly, the damage patterns of sandy soil strata under different conditions were found. Li et al. [26] through numerical simulation and theoretical analysis, assessed the excavation face stability of a shield tunnel in saturated soils under steady seepage flow conditions and obtained an analytical solution for the hydraulic head distribution ahead of the tunnel face in homogeneous and isotropic ground. Zhou et al. [27] investigated the stability of a shield tunnel face under the water table induced by the presence of insufficient supporting pressure, and the parameter analysis indicated that the groundwater seepage had a significant effect on the range of the failure. Xue et al. [28] used Abaqus software to simulate the instability of the excavation face caused by the smaller support pressure of the excavation face, and concluded that the support force of the excavation face was an important factor related to the ground surface deformation. Zhang et al. [29] studied the influence of water pressure seepage on the stability of a large-diameter shield tunnel in soft clay, indicating that the seepage force was a significant factor. Ma et al. [30], Cheng et al. [31], and Liu et al. [32] applied the strength reduction method to the stability analysis of shield tunnel excavation; accordingly, they deduced that the friction angle, the cohesion force, the support pressure of the excavation face and the water level within the soil have a significant influence on the safety of the excavation face. However, there was no discussion on the effect of the thickness of the equivalent layer.

Zhang [33] et al. analyzed the surface deformation of the tunnel by the equivalent layer method and analyzed the sensitivity of the surface deformation to the parameters of the equivalent layer, and they concluded that the larger the thickness, the larger the surface deformation. However, only the surface subsidence was calculated in their analysis, and the influence of the support pressure on the excavation surface was not considered. In actual construction, the shield tail gap and the disturbance zone of grouting behind the tunnel wall are influencing factors in causing surface deformation and stability of the excavation. However, quantifying these factors individually during construction is challenging work. By generalizing them into an equivalent layer, the actual soil layers and grouting conditions behind the lining can be replaced while maintaining unchanged surface deformation.

This study employs a numerical model to investigate the stability of shield tunnel excavation [34], and the validation is verified in terms of seepage field and plasticity calculations. Then, the computational methods are applied to an example of a shield tunnel to verify the surface subsidence pattern. Furthermore, different ultimate support pressure ratios for excavation faces are obtained under varying water level depths, thicknesses of the equivalent layer, diameters of the tunnel, internal frictions, and tunnel burial depths. Finally, a collective discussion is performed on the stability of the excavation of the shield tunnel. These findings provide a theoretical basis for setting the support pressure of excavation faces and controlling surface subsidence in practical dynamic quality control of submarine tunnels.

2. Numerical Modeling and Validation of Excavation Instability

2.1. Presentation of the Calculation Method

The fluid–solid coupling method involves the modeling of fluid and solid mechanics to account for the effects of groundwater. Firstly, a seepage analysis is conducted to store the pore water pressure and total head at each node. Next, the water head gradients at each node are calculated based on the total head values, and the computed seepage forces are stored as nodal forces. Finally, the obtained seepage forces from the seepage analysis are transferred to the stress module as force boundary conditions.

In the fluid–solid coupling analysis, the soil parameters of effective stresses are adopted by the consolidated undrained shear test of soil. The initial horizontal earth pressures are calculated using the water–soil partitioning method. The calculation formulas are expressed as follows [27,28]:

$$\sigma_0 = \gamma_w(L + h) + K_0\gamma' h \tag{1}$$

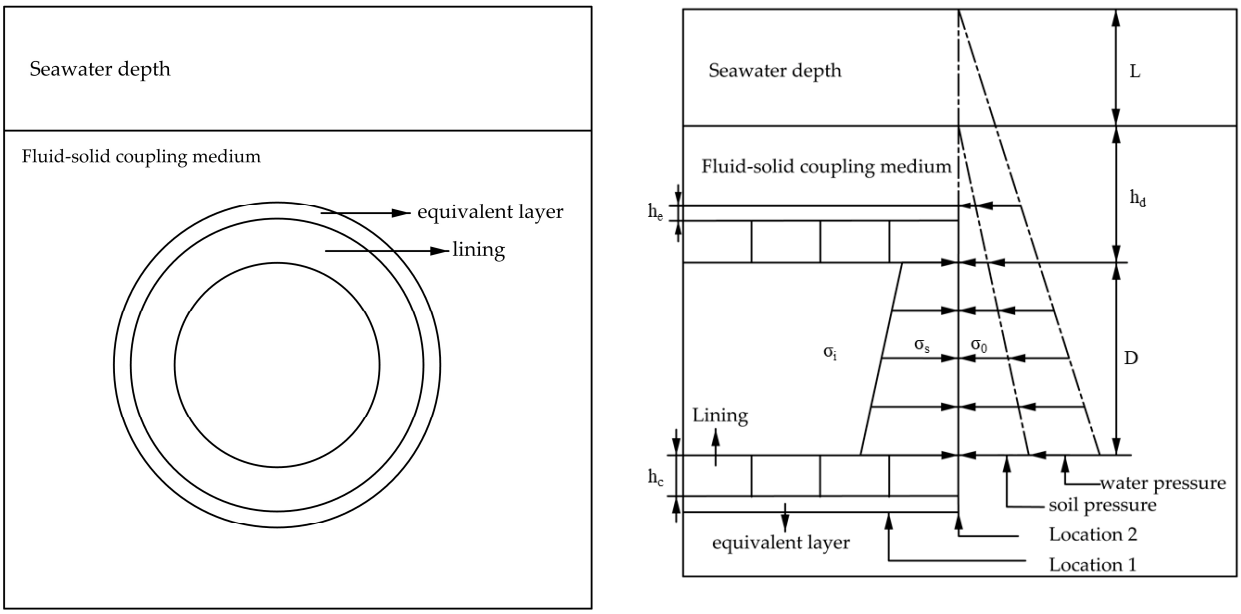
$$\gamma' = \gamma_s - \gamma_w \tag{2}$$

where σ_0 is the initial horizontal earth stress; h denotes the depth of soil layer; γ_w is saturated unit weight; L is water depth; γ' is the floating weight of soil; γ_s is the saturated weight of soil; and K_0 is coefficient of the earth pressure at rest.

Assumed that the supporting force of the tunnel excavation surface σ_i is in the form of a trapezoidal distribution, as shown in Figure 1b. Introducing the support pressure ratio:

$$\sigma_i = \lambda\sigma_0 \tag{3}$$

where σ_i is the stress value of the excavation surface support, and it is applied in the range of $h_d \leq h \leq (h_d + D)$; λ denotes the supporting pressure ratio; h_d is the distance from the top surface of the soil to the top edge of the excavation; and D is the diameter of the excavated surface.



(**a**) (**b**)

Figure 1. Schematic diagram of a shield tunnel using the equivalent layer method: (**a**) Cross-sectional diagram; (**b**) Longitudinal profile illustration.

In practical engineering, the lining is applied to the working face in each step of the excavation; that is, each segment's horizontal distance is instantaneously completed. When the shield moves from position 1 to position 2, the lining also extends from position 1 to position 2. Because an equivalent layer can replace the actual soil layer around the lining, the equivalent layer surrounding the lining consequently extends to position 2, as illustrated in Figure 1.

This study assumes the shield tunnel is at a standstill. By gradually reducing the excavation face supporting pressure ratios, the stabilities of tunnel excavation are calculated under the fluid–solid coupling conditions. The location of the center point of the tunnel is the point in the middle of the tunnel excavation surface, and the displacement of this point is measured by the domain point probe in the software. The flowchart of the numerical calculation for simulating the instability of the excavation surface is shown in Figure 2. The relationship curve between the horizontal displacements at the center point of the excavation face and the supporting pressure ratios can be depicted by the numerical method. As the support pressure ratio decreases, the horizontal displacement of the center point gradually increases. Once there is a slight change in the supporting pressure ratio and the horizontal displacement of the center point does not converge or sharply increase, it indicates instability and failure of the excavation face.

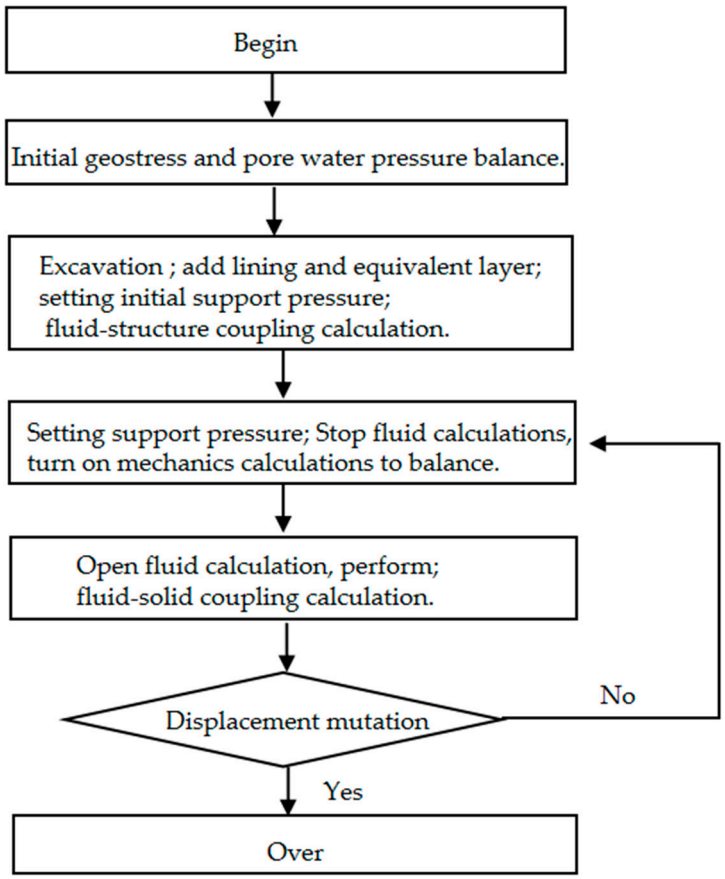


Figure 2. The flowchart of the numerical calculation for simulating the instability of the excavation surface.

2.2. Validation of Calculation Model

2.2.1. Cross-Sectional Plain Model Validation

For comparison of the numerical results by He et al. [35], a numerical model was established using COMSOL for flow–solid coupling analysis, in which the Mohr–Coulomb model was employed. The geometric boundary size of the numerical model is 80 m in length and 60 m in width, with a tunnel with a diameter of 6.28 m at the center. Figure 3

shows that the subsidence range (width) and ground deformation of the numerical results are in good agreement, indicating a consistent distribution pattern. This indicates that the presented numerical calculation scheme is suitable for analyzing the convergence pattern of shield tunnel deformation. Thus, the accuracy of the fluid–solid coupling calculation results in the cross-sectional plain model of this paper is confirmed.

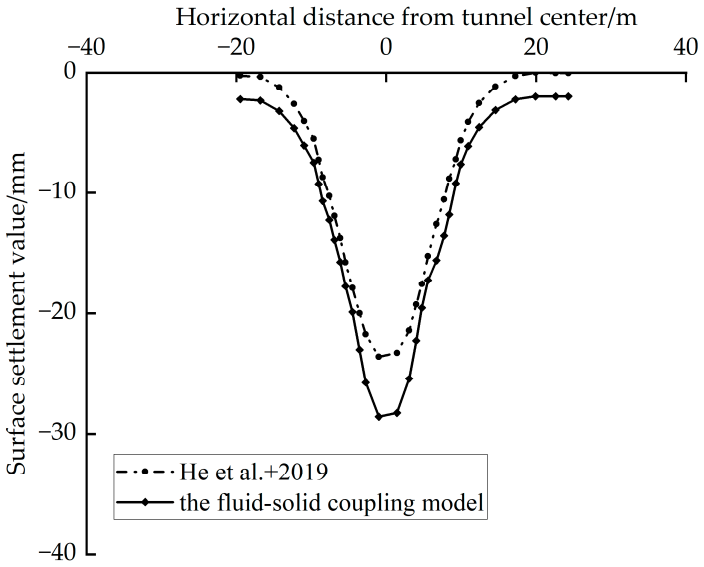


Figure 3. Relationship between surface displacement and tunnel center distance of a shield tunnel in an upper soft and lower hard stratum [35].

2.2.2. Validation of Longitudinal Plain Model

For comparison of the numerical conducted by Kang et al. [36], a numerical model was developed using COMSOL. The geometric boundary size of the model is 50 m in length and 50 m in depth, with a tunnel with a diameter of 10 m and a burial depth of 10 m at the center. Figure 4 shows the comparison of the horizontal displacement diagram of the center point of the tunnel excavation front, and it can be shown that the results of the present numerical model agree well with that calculated by Kang's calculation model.

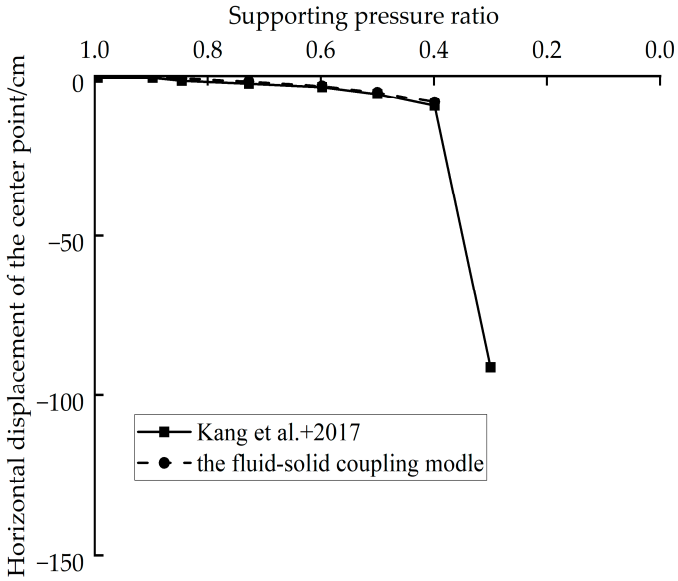


Figure 4. Horizontal displacement of excavation surface center point under different support pressure ratios [36].

2.2.3. Verification for Engineering Instance

1. Project Overview

The shield tunnel with a cross-sectional diameter of 13.46 m was employed by an underwater tunnel project using the slurry balance method, whose outer and inner diameter and wall thickness of the tunnel lining segments are 13.00 m, 11.90 m, and 0.55 m, respectively. This particular tunnel section traverses from a predominantly soft stratum to a weakly weathered rock formation. The primary soil layers of the tunnel cross-section from top to bottom are as follows: mixed fill, silt clay, clay, and weathered tuff. The mechanical parameters of the soil and tunnel segment materials are provided in Table 1.

Table 1. Calculated material parameters.

Stratigraphic Type	Density/kN·m^{-3}	Young's Modulus/MPa	Poisson's Ratio	Angle of Internal Friction	Cohesion	Stratigraphic Number
mixed fill	18	80	0.35	18	28	2.8
silty clay	18	4.6	0.34	9.3	17.2	22.2
clay	17.5	12	0.3	10.8	18.8	10.8
weathered tuff	22	500	0.2	17.3	48	36.2
lining	24.5	34,500	0.17			

2. Numerical model

A cross-sectional numerical model, with geometric sizes of 60 m × 70 m, is established using finite element software. The diameter and soil depth of the tunnel are 13 m and 20.8 m, respectively. The soil layers are composed of a composite formation with a soft upper and a hard lower layer. The Mohr–Coulomb (M-C) model is adopted to describe the constitutive behavior of soil, and the groundwater flow follows Darcy's law. The upper boundary of the model is set as a free surface, while the left and right boundaries and the bottom boundary have normal and fixed constraints, contrastingly. In practical engineering, some effective anti-seepage measures are typically implemented during the underwater shield tunnel construction; therefore, the tunnel excavation face and lining structure are set as impermeable boundaries. By varying the supporting pressure, the excavation face displacements of the tunnel are numerically obtained.

3. Equivalent layer

The equivalent layer is the shield tail gap and the disturbance zone of grouting behind the tunnel wall. The thickness of the equivalent layer is not equal to the theoretical value of the shield tail gap. If the soil behind the tunnel wall is relatively hard and only produces a slight displacement towards the shield tail gap, then the thickness of the equivalent layer should be slightly less than the theoretical value of the shield tail gap. However, while the soil behind the tunnel wall is soft, it moves quickly and fills the shield tail gap after the lining exits the shield tail, resulting in the thickness of the equivalent layer being greater than the theoretical value of the shield tail gap. Hence, Zhang et al. [33] proposed that the thickness of the equivalent layer can be taken as the following formula:

$$\delta = \eta A \tag{4}$$

where A represents the apparent shield tail gap, which is half of the difference between the outer diameter of the shield and the lining (m). η is a coefficient, and the range values from 0.7 to 2.0. For shield tunnels in different soil types, the values of η are hard clay, 0.7 to 0.9; dense sand, 0.9 to 1.3; loose sand, 1.3 to 1.8; and soft clay, 1.6 to 2.0.

Since the material in the equivalent layer is a mixture of soil and cement slurry, its elastic modulus is between that of soil and cement, which can be approximately replaced by the compression modulus of cementitious soil. Although the range of Poisson's ratio

is limited and has little influence on the ground deformation, the Poisson's ratio for the equivalent layer is taken as 0.2, which is typically referred to as the cemented soil. The calculation parameters are summarized in Table 2.

Table 2. Material parameters of the equivalent layer.

Materials	Young's Modulus/MPa	Poisson's Ratio	Thickness/cm
equivalent layer	1	0.2	5

4. Analysis of Surface Subsidence

Figure 5 shows the surface subsidence map obtained from the present model using COMSOL Multiphysics software. According to the monitoring results of surface subsidence in the field test, the maximum variation in surface subsidence for the shield tunnel is 29 mm.

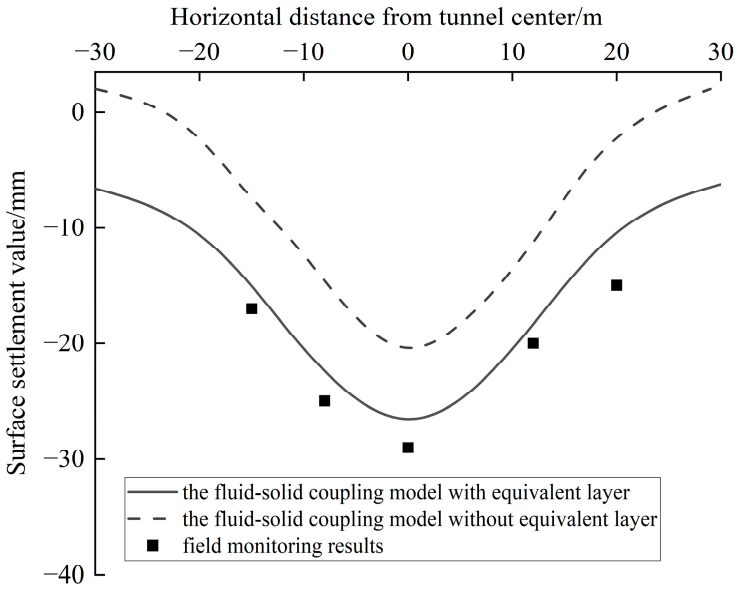


Figure 5. Ground surface subsidence displacement map.

As seen in Figure 5, the maximum surface subsidence without the equivalent layer under the fluid–solid coupling model is approximately 20 mm, which significantly differs from the actual monitoring value of 29 mm. For comparison, the maximum surface subsidence with the equivalent layer under the fluid–solid coupling model is approximately 26 mm, which is close to the actual monitoring value. It is obvious that considering the equivalent layer is more suitable to describe this excavation process.

3. Sensitivity Analysis of Factors Influencing the Stability of Tunnel Excavation

The stability of tunnel excavation is related to the water level depth, the thickness of the equivalent layer, the tunnel diameter, the internal friction angle, and the tunnel burial depth of soil. The effects of these factors on the ultimate supporting pressures of tunnel excavation are illustrated in this section, as well as the deformation, instability, and failure state of the surrounding ground. The dimensions of the calculated model are illustrated in Figure 6. The geological conditions and parameters of the tunnel are consistent with those in Table 1.

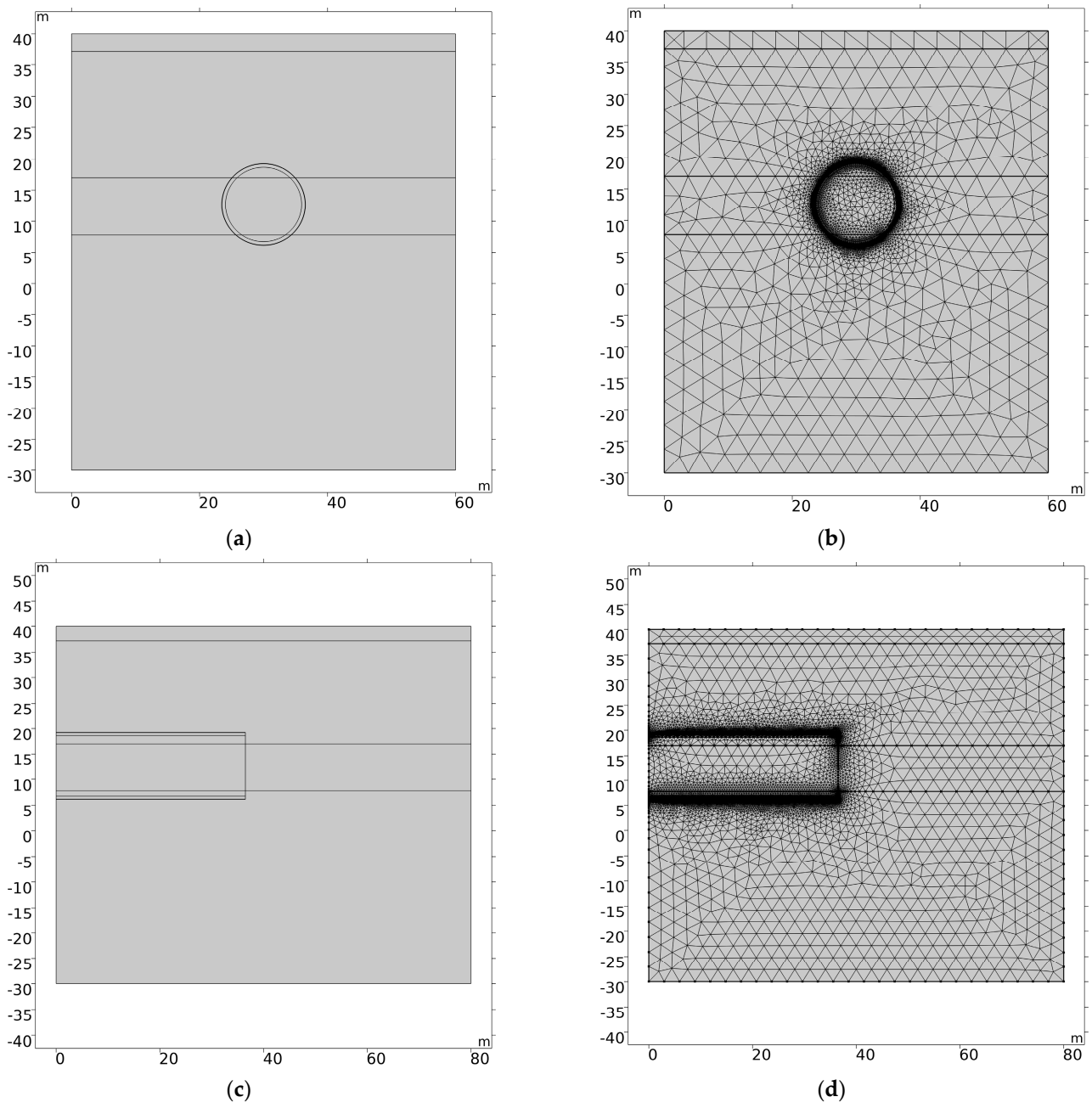
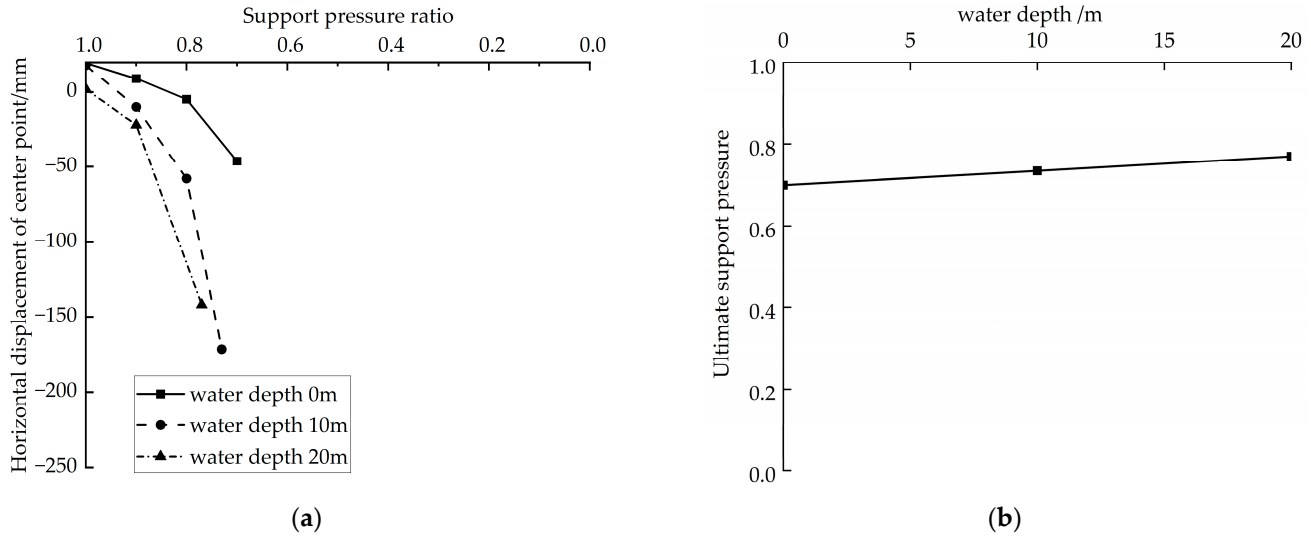


Figure 6. Numerical simulation calculation model and grid diagram: (**a**) Cross-sectional model; (**b**) Cross-sectional mesh profile graph; (**c**) Longitudinal profile model; (**d**) Schematic diagram of longitudinal section grid.

3.1. Effect of Water Depth on the Tunnel

3.1.1. Determination of the Ultimate Support Pressure Ratio

From the relationship curves in Figure 7, similar patterns for horizontal displacements and supporting pressure ratios under different water depths are shown. With the increase in water level, the maximum supporting pressure ratio for the destabilization of the excavation surface increases; that is, the stability of the excavation surface is significantly reduced. Under the condition of the same support pressure ratio, the higher the water level, the larger the displacement and the more obvious the increasing trend.

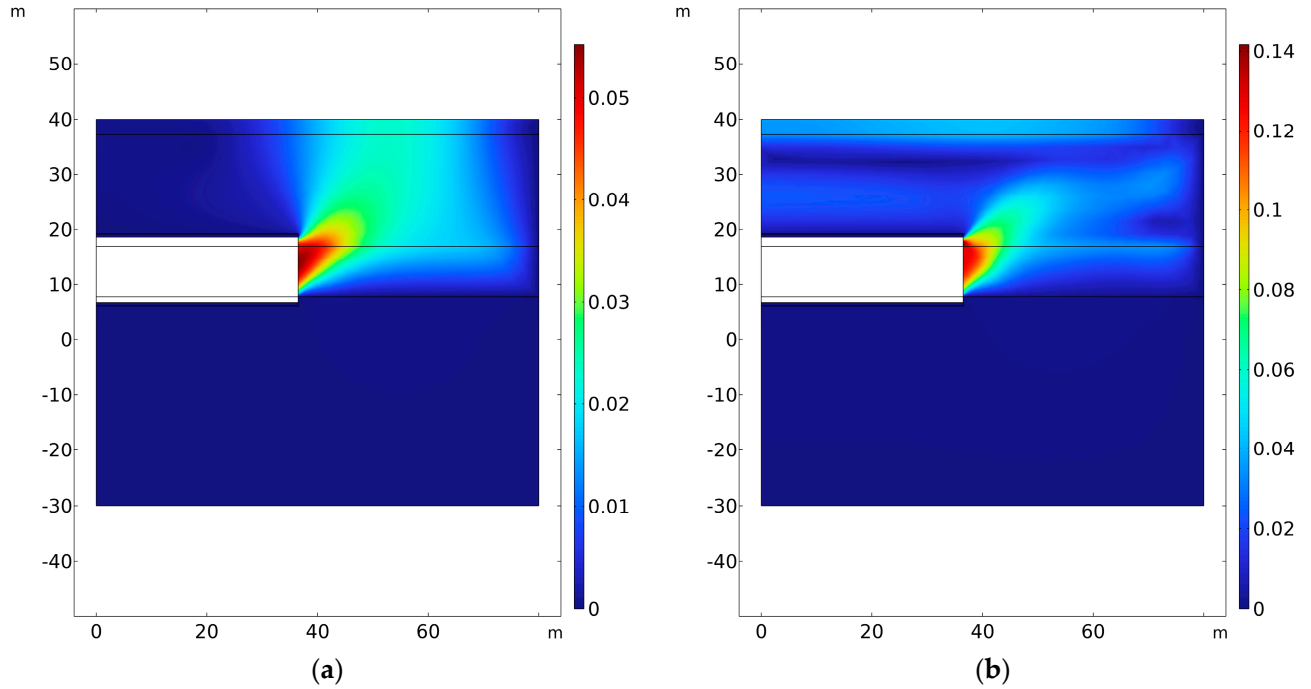


(**a**) (**b**)

Figure 7. Relationship between support force of excavation face and horizontal displacement of excavation face under different water levels: (**a**) Relationship curve between support ratio and horizontal displacement of excavation surface; (**b**) Relationship curve between water level and ultimate support ratio of excavation surface.

3.1.2. Destabilization Damage Mode

Figure 8 shows the displacement distribution clouds of the shield tunnel at water levels of 0 and 20 m, respectively. As seen from the above figure, the seawater level has a greater influence on the form of destabilization damage at the excavation surface. As the water level decreases, the tendency of the chimney-shaped collapse to the surface in front of the excavation face gradually decreases.



(**a**) (**b**)

Figure 8. Displacement clouds of excavation faces at the center points for different water levels: (**a**) Displacement cloud of water level 0 m; (**b**) Displacement cloud of water level 20 m.

3.2. Effect of the Thickness of the Equivalent Layer

3.2.1. Determination of the Ultimate Support Pressure Ratio

From the relationship curves in Figure 9, it can be observed that with the different variations in the support force of the excavation surface, the different thicknesses of equivalent layers exhibit similar patterns. When the support force of the excavation surface is less than the ultimate support force, the tunnel excavation surface is prone to collapse, resulting in large surface deformation. The thickness of the equivalent layer has a significant impact on surface displacement. As the thickness of the equivalent layer increases, the ultimate support ratio of the excavation surface increase as well, and the surface displacement increases almost linearly with the thickness of the equivalent layer.

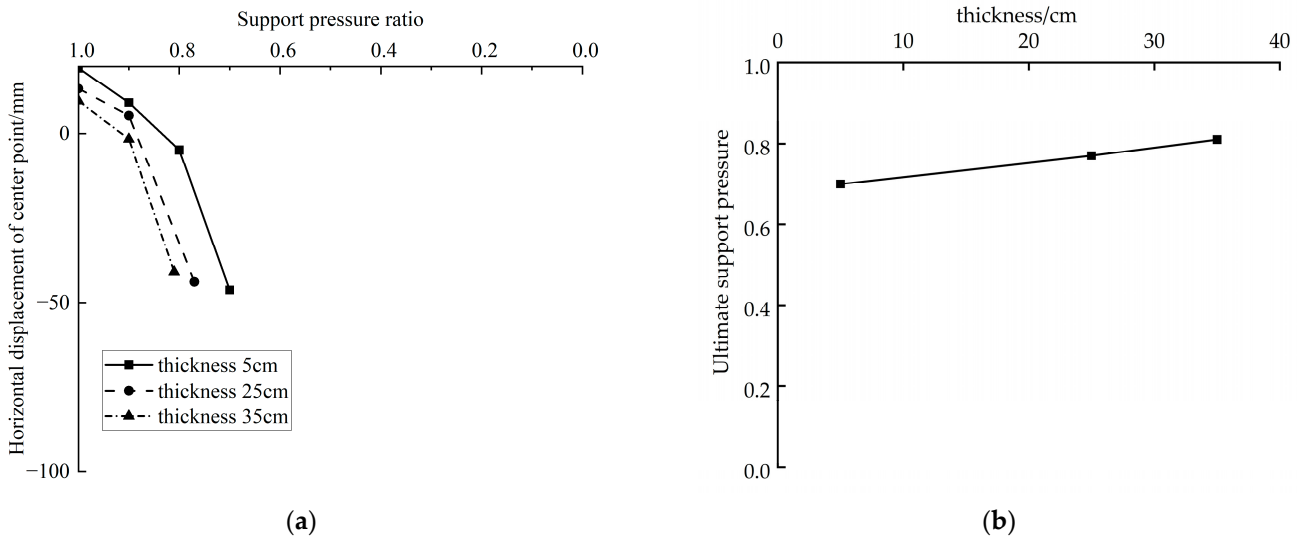


Figure 9. Relationship between the support force of the excavation face and the horizontal displacement of the center of the excavation face under different thicknesses of equivalent layer: (**a**) Relationship curve between support ratio and horizontal displacement of excavation surface; (**b**) Relationship curve between water level line and ultimate support ratio of excavation surface.

The thickness of the equivalent layer is related to the amount of grouting and the extent range of disturbance to the surrounding soil during construction. Therefore, it is essential to avoid over-excavation and disturbance to the surrounding soil during tunnel construction in order to reduce the thickness of the equivalent layer and control the displacement of the ground.

3.2.2. Destabilization Damage Mode

Figure 10 shows the displacement distribution clouds of the shield tunnel at the thickness of equivalent layers of 5 and 35 cm, respectively. Seen from the contour maps, the damage pattern of the excavation surface exhibits a wedge-shaped region in the front of the excavation surface and a chimney-shaped region at the top of the failure zone, thus reaching an unstable state.

3.3. Effect of Tunnel Diameter

3.3.1. Determination of the Ultimate Support Pressure Ratio

From the relationship curves in Figure 11, different tunnel diameters exhibit similar patterns in the variation in supporting pressure of the excavation face. As the supporting pressure decreases, the horizontal displacement at the center point of the tunnel gradually increases. When the supporting pressure of the excavation surface is less than the ultimate supporting pressure, the tunnel excavation surface is prone to collapse, leading to significant excavation surface deformation. There is a roughly linear relationship between

tunnel diameter and the ultimate supporting stress of the excavation surface, while there is a limited impact on the excavation surface for smaller tunnel diameters under the variation in supporting pressure of the excavation surface. However, for larger tunnel diameters, such as 20 m, the supporting pressure of the excavation surface has a significant effect on the tunnel excavation surface.

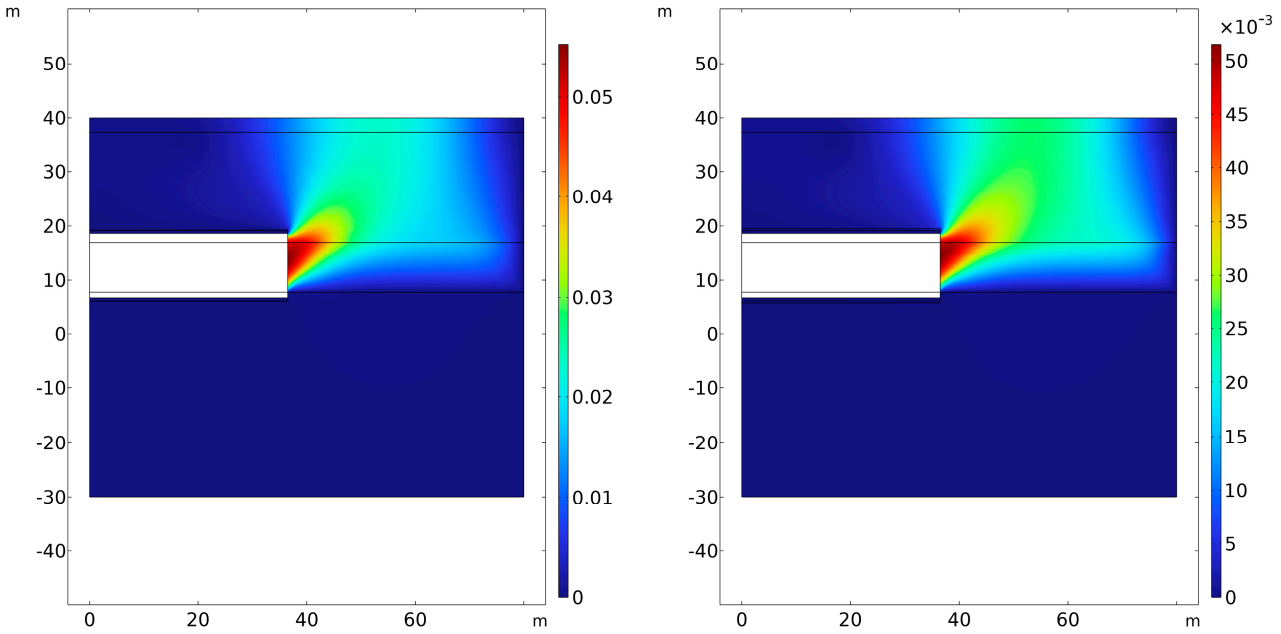


Figure 10. Displacement clouds of the equivalent layer at different thicknesses: (**a**) Displacement cloud of thickness 5 cm; (**b**) Displacement cloud of thickness 35 cm.

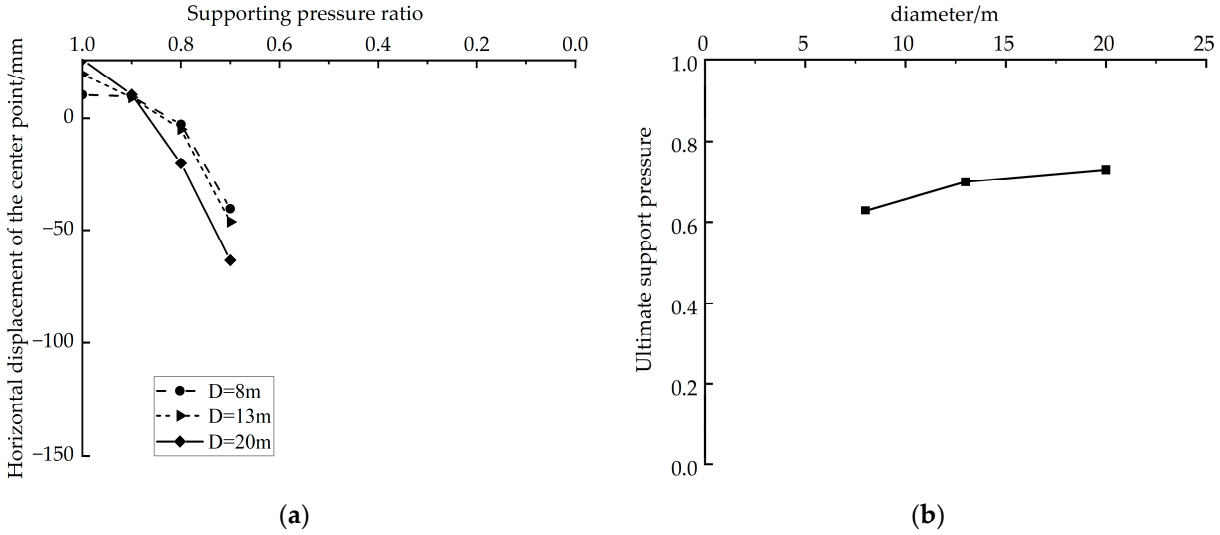


Figure 11. Relationship between different support pressure ratios and horizontal displacement of excavation face under different diameters: (**a**) Relationship curve between support ratio and horizontal displacement of excavation surface; (**b**) Relationship curve between water level line and ultimate support ratio of excavation surface.

3.3.2. Destabilization Damage Mode

Figure 12 shows the displacement distribution clouds of the shield tunnel at the diameters of 8 and 20 m, respectively. Under the influence of underground seepage, even

in the case of small tunnels with a diameter of 8 m, when the support force is less than the ultimate support force, there will be a significant effect on the tunnel excavation surface.

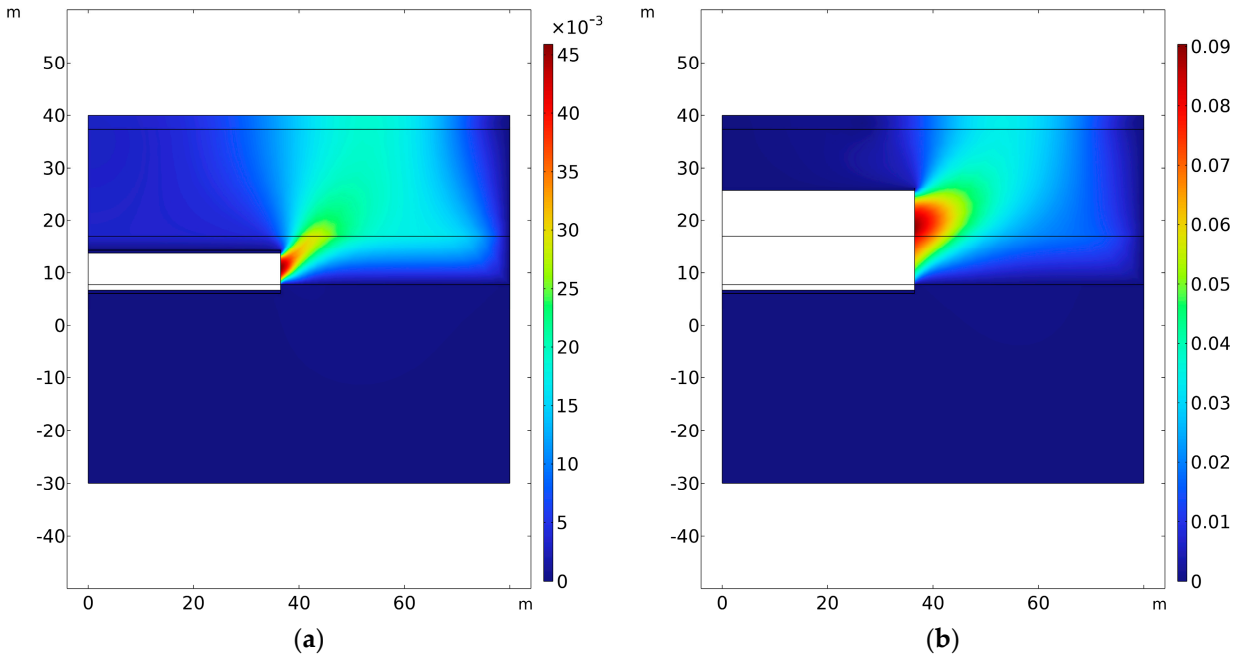


Figure 12. Displacement clouds at different diameters: (**a**) Displacement cloud of diameter 8 m; (**b**) Displacement cloud of diameter 8 m.

3.4. Effect of Internal Friction Angle

The effects of the internal friction angle on the stability of the excavation surface are investigated for a shield tunnel of a composite stratum with an upper soft soil layer and a lower hard soil layer

3.4.1. Determination of the Ultimate Support Pressure Ratio

Based on Figure 13, when the support force approaches the static earth pressure, the displacements are relatively small for different friction angles, and the effect of the internal friction angle on the excavation face deformation is not very pronounced. However, when the support force further decreases, and the deformation curve of the excavation face enters the second stage, the influence of the internal friction angle on the deformation becomes more prominent. Under the same support force, as the internal friction angle of the soil increases, the deformation of the excavation continuously decreases. With the increase in the internal friction angle of the soil, the ultimate support force of the excavation surface decreases.

3.4.2. Destabilization Damage Mode

Figure 14 shows the displacement distribution clouds of the shield tunnel at the friction angles of 8° and 20°, respectively. As seen from the contour maps, with the increase in friction angle, the soil displacement gradually decreases. And, the inclination of the wedge in front of the excavation face gradually decreases as the friction angle of the soil increases.

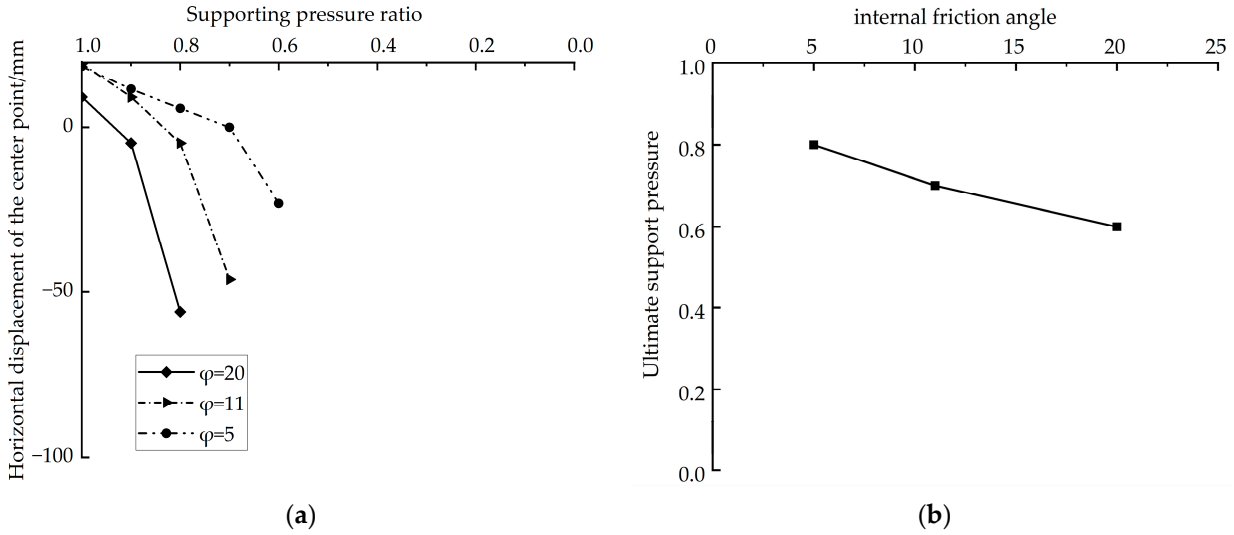


Figure 13. Relationship between the support force of the excavation face and the horizontal displacement of the center of the excavation face under different internal friction angles: (**a**) Relationship curve between support ratio and horizontal displacement of excavation surface; (**b**) Relationship curve between water level line and ultimate support ratio of excavation surface.

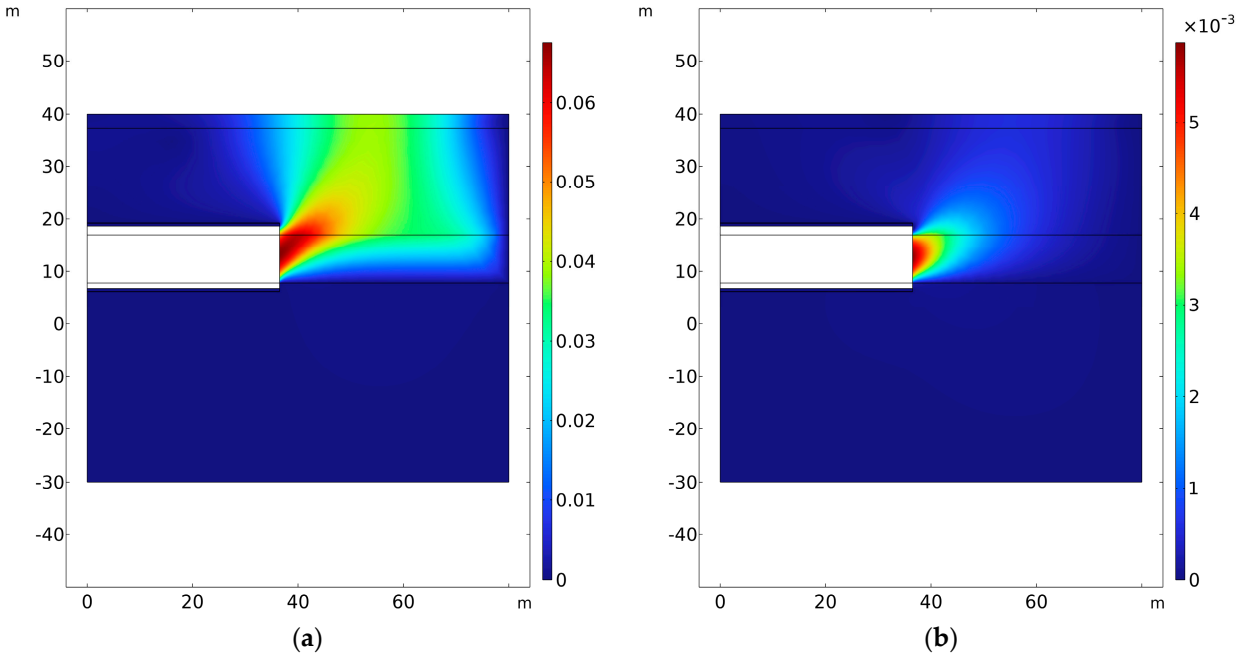
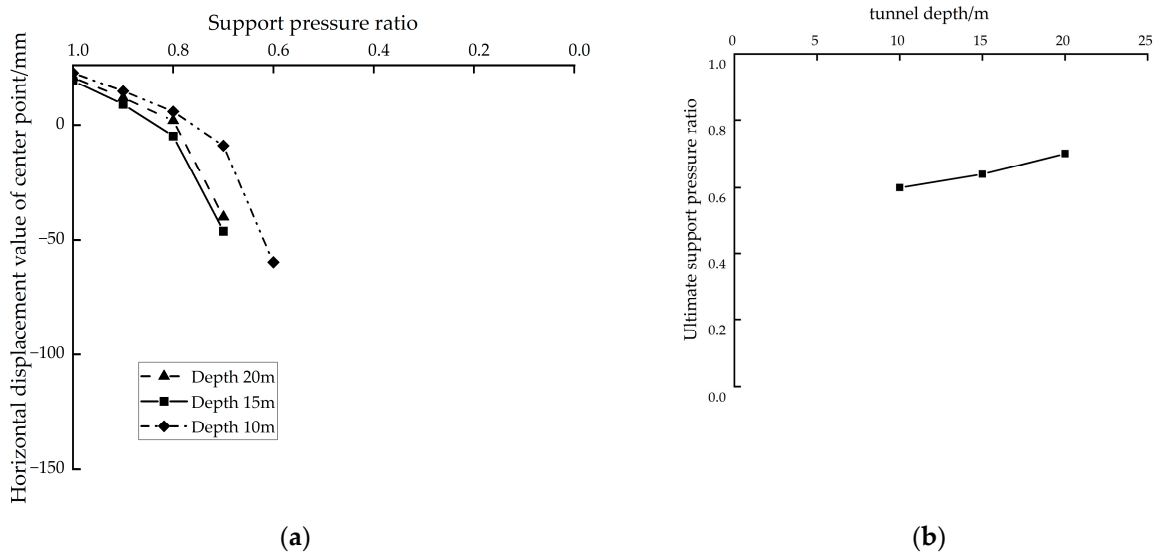


Figure 14. Displacement clouds at different diameters: (**a**) Displacement cloud of internal friction angle 8°; (**b**) Displacement cloud of internal friction angle 20°.

3.5. Effect of Tunnel Burial Depth

3.5.1. Determination of the Ultimate Support Pressure Ratio

From the relationship curves in Figure 15, the shapes of the curves with the changes in burial depth are basically the same, the horizontal displacement at the center point of the excavation face gradually increases with the decrease in the support ratio, and the displacement suddenly increases faster after the limit support ratio. As the burial depth of the tunnel increases, the ultimate support ratio at the excavation face also increases. For the cases of the same support ratios, the displacement of the soil at the excavation surface increases with the burial depth of the tunnel.

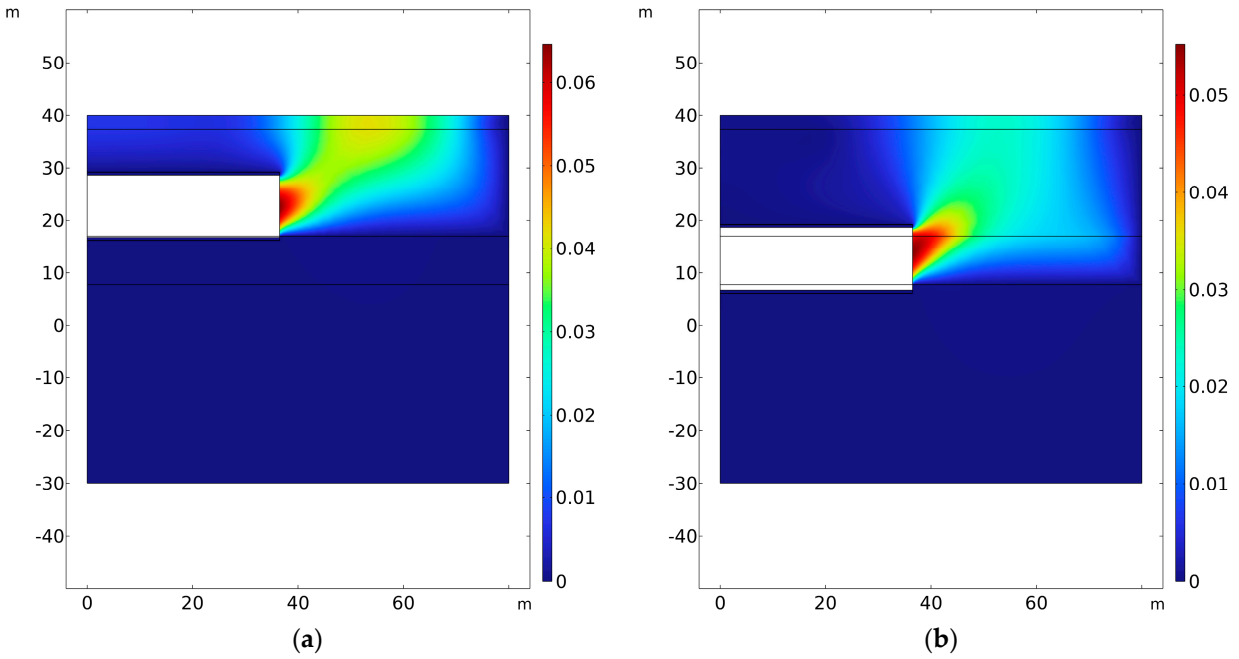


(**a**) (**b**)

Figure 15. Relationship between different support pressure ratios and horizontal displacement of excavation face under different tunnel burial depths: (**a**) Relationship curve between support ratio and horizontal displacement of excavation surface; (**b**) Relationship curve between water level line and ultimate support ratio of excavation surface.

3.5.2. Destabilization Damage Mode

From the displacement cloud Figure 16, it can be seen that the front of the excavation is wedge-shaped in the damaged area and the displacement is funnel-shaped in the upper area. The damage of the excavation develops from the excavation face up to the ground surface. The damage mode of excavation has a great relationship with the burial depth of the tunnel; when the tunnel depth is shallow, the damaged area can be developed to the ground surface, and with an increase in burial depth, it becomes more and more difficult to develop to the ground.



(**a**) (**b**)

Figure 16. Displacement clouds at different depths of 10 m: (**a**) Displacement cloud of diameter 8 m; (**b**) Displacement cloud of depth 20 m.

4. Discussion

The support pressure on the excavation surface during shield construction of submarine tunnels is a key factor affecting the stability of the excavation and surface subsidence, and a reasonable determination of its value is an important problem solved in this paper. Taking the seepage force into account, and, accordingly, the effective stresses in the soil, the fluid–solid coupling model is employed in the simulation of the excavation of a submarine shield tunnel. During the actual excavation, it was difficult to simulate the excavation rigorously, especially for the shield tail void, the disturbance of the soil behind the tunnel wall, the treatment of the grouting layer, etc. We used the equivalent layer to replace this thin layer, which can better reflect the actual excavation deformation. In consideration of the fluid–solid coupling effect and the equivalent layer on the stability of the excavation face of the submarine shield tunnel, this paper yields some useful results.

1. When the excavation face is destabilized, the sliding body in the front of the excavation is wedge-shaped, and there is chimney-shaped damage on the whole area. Zhu et al. [37] investigated the method of determining the ultimate supporting forces of the excavation face in the presence of groundwater and the damage modes of the excavation face in sandy soil stratum through FLAC3D software. The results obtained in their paper are approximately the same as the present one. Moreover, compared with the seepage-stress pseudo-coupling calculation model in the literature, this model in the present paper considers the composite stratum and the fluid–solid coupling effect, which makes the results have practical significance in engineering.
2. By generalizing the shield tail gap and the grouting disturbance zone behind the tunnel wall into the equivalent layer, the actual soil layers and grouting conditions behind the lining can be considered. This method can better simulate the destructive effect of the deformation of the excavation, and coincide with the on-site monitoring results, so it can better reflect the destructive mechanism of the deformation of the tunnel excavation surface.
3. The excavation displacement and the ultimate support ratio increase linearly with the increase in the thickness of the equivalent layer, water depth, and diameter. However, the ultimate support ratio at the excavation face decreases with the increase in the internal friction angle of the soil. These conclusions are basically consistent with the conclusions of Zhang et al. [33], Kang, et al. [36], and Zhu et al. [37] Most of the articles have not discussed the thickness of the equivalent layer, which is related to the amount of grouting during construction and the extent of the disturbance of the surrounding soil behind the lining wall. Therefore, it is necessary to avoid over-excavation and disturbing the surrounding soil during tunnel construction to reduce the thickness of the equivalent layer in order to control the displacement of the ground surface.

5. Conclusions

In this paper, the stability of the excavation face of a subsea tunnel is studied using a numerical simulation method, taking into account the fluid–solid coupling effect. The following conclusions are obtained:

1. The destabilization of the excavation face of a submarine shield tunnel will lead to the extension of soil deformation to the surface, with a wedge shape in front of the excavation face and a chimney shape at the top of the damaged area.
2. Through the numerical simulation of the submarine tunnel using the fluid–solid coupling model, it is concluded that the maximum surface subsidence value is approximately 26 mm, which is larger than the value calculated for plasticity, closer to a field monitoring value of 29 mm. The soil near the excavation surface experiences significant disturbance, resulting in the instability of the excavation face.
3. Taking into account the effect of the equivalent layer on the subsea shield tunnel, it can be concluded that the equivalent layer can more objectively reflect the comprehensive effects of the factors that are difficult to quantify. The surface subsidence is approximately 26 mm with the equivalent layer, and 20 mm without the equivalent layer, with

the equivalent layer closer to the actual monitoring value of 29 mm. Furthermore, the thickness of the equivalent layer has a significant influence on surface deformation. The greater the thickness, the greater the surface deformation.

4. The numerical results show that the water depth, tunnel diameter, internal friction angle, and tunnel depth have significant effects on the ultimate supporting pressure ratio. With the increases in the water depth, the burial depth and the tunnel diameter, the ultimate supporting pressure ratios at the excavation face will continue to increase. While as the internal friction angle increases, the supporting pressure ratio at the excavation face continues to be reduced.

Author Contributions: Conceptualization, Q.W. and Q.L.; methodology, Q.W.; software, J.Z.; validation, Q.W., Q.L. and J.Z; formal analysis, Q.W., Q.L. and J.Z; investigation, Q.W., Q.L. and Z.Z.; resources, J.Z; data curation, Q.W.; writing—original draft preparation, Q.W., Q.L. and Z.Z.; writing—review and editing, Q.W., Q.L. and Z.Z.; visualization, Q.W. and Z.Z.; supervision, Q.L.; project administration, Q.W. and Q.L. All authors have read and agreed to the published version of the manuscript.

Funding: This research was funded by the Balanced Architecture Research Center of Zhejiang University under grant number K-H20203389C.

Institutional Review Board Statement: Not applicable.

Informed Consent Statement: Not applicable.

Data Availability Statement: Not applicable.

Conflicts of Interest: The authors declare no conflict of interest.

References

1. Chambon, P.; Corte, J.F. Shallow tunnels in cohesionless soil: Stability of tunnel face. *J. Geotech. Eng.* **1994**, *120*, 1148–1165. [CrossRef]
2. Wang, Z.; Wang, Y.; Feng, D. Wedge Instability Model Improvement of Shield Tunnel Excavation Face under Inclined Surface. *Adv. Civ. Eng.* **2021**, *2021*, 6694730. [CrossRef]
3. Song, W.; Zhang, P.; Du, X. Evaluation of judging criteria on the limit support pressure of shield excavation face in sandy stratum. *Arab. J. Geosci.* **2022**, *15*, 383. [CrossRef]
4. Schweiger, H.F.; Pottler, R.K.; Steiner, H. Effect of seepage forces on the shotcrete lining of a large undersea cavern. In Proceedings of the International Conference on Computer Methods and Advances in Geomechanics, Cairns, Australia, 6–10 May 1991; pp. 1503–1508.
5. Zhang, F.; Gao, Y.; Wu, Y. Face stability analysis of large-diameter slurry shield-driven tunnels with linearly increasing undrained strength. *J. Tunn. Undergr. Space Technol.* **2018**, *78*, 178–187. [CrossRef]
6. Li, X.; Jia, C.; Zhao, H. Investigation on the influence of the Bohai Sea Geological Environment on the submarine stratum stability based on data mining: An intelligent prediction model. *Environ. Sci. Pollut. Res.* **2023**, *30*, 11617–11633. [CrossRef] [PubMed]
7. De Buhan, P.; Cuvillier, A.; Dormieux, L. Face stability of shallow circular tunnels driven under the water table: A numerical analysis. *Int. J. Numer. Anal. Methods Geomech.* **1999**, *23*, 79–95. [CrossRef]
8. Soranzo, E.; Tamagnini, R.; Wu, W. Face stability of shallow tunnels in partially saturated soil: Centrifuge testing and numerical analysis. *Geotechnique* **2015**, *65*, 454–467. [CrossRef]
9. Duan, J.; Li, C.; Jin, J. Modal Analysis of Tubing Considering the Effect of Fluid–Structure Interaction. *Energies* **2022**, *15*, 670. [CrossRef]
10. Hu, Q.; Tang, Y.; Ding, Z. Study on the Stability of a Transition Section from Soft to Hard Surrounding Rock Based on the Solid-Fluid Coupling Effect. *Adv. Civ. Eng.* **2020**, *2020*, 6964151. [CrossRef]
11. Huang, Z.; Wu, J.; Zhang, Y. Analysis of the Stability of the Shield Tunnel Excavation Face Considering Fluid-Solid Coupling Effect. *Mod. Tunn. Technol.* **2018**, *55*, 61–71.
12. Ahmed, M.; Iskander, M. Evaluation of tunnel face stability by transparent soil models. *Tunn. Undergr. Space Technol.* **2012**, *27*, 101–110. [CrossRef]
13. Atkinson, J.H.; Potts, D.M. Stability of a shallow circular tunnel in cohesionless soil. *Geotechnique* **1977**, *27*, 203–215. [CrossRef]
14. Hisatake, M.; Eto, T.; Murakami, T. Stability and failure mechanisms of a tunnel face with a shallow depth. In Proceedings of the 8th ISRM Congress, Tokyo, Japan, 25–29 September 1995; OnePetro: Richardson, TX, USA, 1995.
15. Anagnostou, G.; Kovári, K. Face stability conditions with earth-pressure-balanced shields. *Tunn. Undergr. Space Technol.* **1996**, *11*, 165. [CrossRef]
16. Anagnostou, G. The contribution of horizontal arching to tunnel face stability. *Geotechnik* **2012**, *35*, 34–44. [CrossRef]

17. Anagnostou, G.; Perazzelli, P. Analysis method and design charts for bolt re-inforcement of the tunnel face in cohesive-frictional soils. *Tunn. Undergr. Space Technol.* **2015**, *47*, 162–181. [CrossRef]
18. Alagha, A.S.N.; Chapman, D.N. Numerical modelling of tunnel face stability in homogeneous and layered soft ground. *Tunn. Undergr. Space Technol.* **2019**, *94*, 103096. [CrossRef]
19. Vermeer, P.A.; Ruse, N.; Marcher, T. Tunnel heading stability in drained ground. *Felsbau* **2002**, *26*, 8–18.
20. Broere, W.; Van Tol, A.F. Influence of infiltration and groundwater flow on tunnel face stability. *Geotech. Asp. Undergr. Constr. Soft Ground* **2000**, *1*, 339–344.
21. Kim, S.H.; Tonon, F. Face stability and required support pressure for TBM driven tunnels with ideal face membrane–Drained case. *Tunn. Undergr. Space Technol.* **2010**, *25*, 526–542. [CrossRef]
22. Mair, R.J.; Taylor, R.N. Bored tunnelling in the urban environment. In Proceedings of the International Conference on Soil Mechanics & Foundation Engineering, Hamburg, Germany, 6–12 September 1997.
23. Kirsch, A. Experimental investigation of the face stability of shallow tunnels in sand. *Acta Geotech.* **2010**, *5*, 43–62. [CrossRef]
24. Lambrughi, A.; Rodriguez, L.M.; Castellanza, R. Development and validation of a 3D numerical model for TBM–EPB mechanised excavations. *Comput. Geotech.* **2012**, *40*, 97–113. [CrossRef]
25. Lü, X.; Zeng, S.; Zhao, Y. Physical model tests and discrete element simulation of shield tunnel face stability in anisotropic granular media. *Acta Geotech.* **2020**, *15*, 3017–3026. [CrossRef]
26. Wei, L.; Zhang, C.P.; Tan, Z.B.; Ma, M.S. Effect of the seepage flow on the face stability of a shield tunnel. *Tunn. Undergr. Space Technol.* **2021**, *112*, 103900.
27. Zhou, Z.; Ling, T.; Huang, F. The Face Stability Analysis of Shield Tunnels Subjected to Seepage Based on the Variational Principle. *Sustainability* **2022**, *14*, 16538. [CrossRef]
28. Xue, F.; Zhang, M. Excavation Face Stability of Shield Tunneling Closely Under Existing Tunnels: Particle Flow Simulation. *Iran. J. Sci. Technol. Trans. Civ. Eng.* **2020**, *44*, 497–506. [CrossRef]
29. Zhang, S.; Cheng, X.; Qi, L.; Zhou, X. Face stability analysis of large diameter shield tunnel in soft clay considering high water pressure seepage. *Ocean. Eng.* **2022**, *253*, 111283. [CrossRef]
30. Ma, S.; Duan, Z.; Huang, Z.; Liu, Y.; Shao, Y. Study on the stability of shield tunnel face in clay and clay-gravel stratum through large-scale physical model tests with transparent soil. *Tunn. Undergr. Space Technol.* **2022**, *119*, 104199. [CrossRef]
31. Cheng, X.; Zhang, S.; Zhou, X.; Xia, P. Parameter analysis of excavation face stability of shield tunnel under high water pressure seepage. *Phys. Chem. Earth* **2022**, *128*, 103218. [CrossRef]
32. Yu, L.; Zhang, D.; Fang, Q.; Cao, L.; Zhang, Y.; Xu, T. Face stability of shallow tunnelling in sandy soil considering unsupported length—ScienceDirect. *Tunn. Undergr. Space Technol.* **2023**, *102*, 8–10.
33. Zhang, Y.; Yin, Z.; Xu, Y. Analysis of surface deformation caused by shield tunneling. *J. Rock Mech. Eng.* **2002**, *21*, 388–392.
34. Ding, W.; Wang, Z.; Huang, X. Study on excavation stability of shallow rectangular shield pipe jacking tunnel. *Arab. J. Geosci.* **2022**, *15*, 691. [CrossRef]
35. He, X.H.; Zhou, C.Z.; Wang, H.B. Study on deformation characteristics of shield tunnel in upper soft and lower hard composite strata. *Mod. Urban Rail Transit* **2019**, *02*, 54–57.
36. Kang, Z.J.; Tan, Y.; Li, J.L. Study on stability of shield tunnel excavation surface based on flow-solid coupling. *Tunn. Constr.* **2017**, *37*, 9.
37. Zhu, Y. *Stability Analysis of Shield Tunnel Excavation Face under Seepage Conditions*; Tianjin University: Tianjin, China, 2023; pp. 8–10.

Disclaimer/Publisher's Note: The statements, opinions and data contained in all publications are solely those of the individual author(s) and contributor(s) and not of MDPI and/or the editor(s). MDPI and/or the editor(s) disclaim responsibility for any injury to people or property resulting from any ideas, methods, instructions or products referred to in the content.